




# FeCoNiCr<sub>0.5</sub>Al<sub>x</sub> High-Entropy Alloys with Dual-Phase Solidification Microstructure and High Compressive Properties

TAO LU <sup>1</sup>, WENKE CHAI,<sup>1</sup> TING DAI,<sup>1</sup> and YE PAN<sup>1,2</sup>

1.—School of Materials Science and Engineering, Jiangsu Key Laboratory of Advanced Metallic Materials, Southeast University, Nanjing 211189, China. 2.—e-mail: panye@seu.edu.cn

FeCoNiCr<sub>0.5</sub>Al<sub>x</sub> high-entropy alloys (HEAs) have been prepared via the self-propagating high-temperature casting method and the phase formation mechanism and related compressive properties systematically investigated. The FeCoNiCr<sub>0.5</sub>Al<sub>x</sub> HEAs showed dual-phase nature but complex as-cast microstructure depending on the Al content. The as-cast microstructure of the FeCoNiCr<sub>0.5</sub>Al<sub>0.8</sub> and FeCoNiCr<sub>0.5</sub>Al<sub>1.0</sub> HEAs was composed of ordered/non-ordered body-centered cubic (BCC) nanocomposite dendrites, network-like interdendritic face-centered cubic (FCC)/BCC eutectics, and plate-like FCC/BCC eutectics. The high compressive properties can be attributed to the eutectics formed both interdendritically and at grain boundaries, which considerably reduce the embrittlement of the interfaces.

## INTRODUCTION

High-entropy alloys (HEAs), which contain multiple principal elements, represent a novel design strategy for high-performance alloys.<sup>1–7</sup> FeCoNiCr-based HEAs are a representative group characterized by a single solid-solution phase with either face-centered cubic (FCC) or body-centered cubic (BCC) structure depending on the fifth principal element, e.g., FeCoNiCrMn (FCC)<sup>8–11</sup> and FeCoNiCrAl (BCC).<sup>12,13</sup> To identify the kind and stability of the solid-solution phase in FeCoNiCr-based HEAs, Zhang et al.<sup>14</sup> proposed a series of solid-solution formulas including the entropy of mixing ( $\Delta S_{\text{mix}}$ ), enthalpy of mixing ( $\Delta H_{\text{mix}}$ ), and atomic-size difference ( $\delta$ ). Guo et al.<sup>15</sup> also adopted the electronegativity difference ( $\Delta\chi$ ) and valence electron concentration (VEC) to predict the formation of different solid-solution phases in equiatomic or nonequiatomic HEAs.

HEAs with an FCC matrix comprising a single solid solution exhibit high ductility but low strength at room temperature, whereas BCC-matrix HEAs exhibit much higher strength but lower ductility.<sup>16–20</sup> Considering this regularity, much effort has been expended in attempts to obtain a trade-off between the strength and ductility of dual-phase

HEAs composed of either two solid solutions or one solid-solution matrix with various ordered intermetallics. He et al.<sup>21</sup> designed a FeCoNiCr HEA alloyed with Ti and Al elements and found that the  $\gamma'$  precipitates with Ni<sub>3</sub>(Ti,Al) structure considerably strengthened the FCC matrix. Yang et al.<sup>22</sup> recently reported that a (Ti,Al)-doped FeCoNi equiatomic alloy showed much higher yield strength and tensile strength of 1 GPa and 1.5 GPa, respectively, while the ductility remained at 50% after fracture. They found a ductile (Ni<sub>43.3</sub>Co<sub>23.7</sub>Fe<sub>8</sub>)<sub>3</sub>(Ti<sub>14.4</sub>Al<sub>8.6</sub>Fe<sub>2</sub>) multicomponent nanoprecipitate homogeneously dispersed in the FCC matrix. Using another method, BCC-matrix HEAs can also be toughened by adjustment of the principal elements, leading to formation of complex phases. Fan et al.<sup>23</sup> found that the compressive strength and ductility of a C-doped AlFeCoNi HEA were 2.4 GPa and 32.6%, respectively, since the as-cast microstructure was composed of B2 dendrites with a nanostructure of interdendrites in which nano L1<sub>2</sub> phases precipitated from the FCC solid solution.

In the work presented herein, a series of FeCoNiCr<sub>0.5</sub>Al<sub>x</sub> HEAs were prepared via the self-propagating high-temperature synthesis method. The compressive properties of the HEAs with different Al element contents depended notably on the as-cast microstructure, which showed a dual-phase nature with a combination of BCC dendrites and FCC

Tao Lu and Wenke Chai have contributed equally to this work.

interdendrites. This work focuses on a discussion of the solidification process and the formation of this dual-phase microstructure.

### EXPERIMENTAL PROCEDURES

FeCoNiCr<sub>0.5</sub>Al<sub>x</sub> HEAs were synthesized using the thermite reaction between Al element and metal oxides Co<sub>2</sub>O<sub>3</sub>, Cr<sub>2</sub>O<sub>3</sub>, Fe<sub>2</sub>O<sub>3</sub>, and NiO according to the designed compositions. Reactant powders of analytical grade with average particle size of 75 μm were supplied by SCRC (Sinopharm Chemical Reagent Co. Ltd., P.R. China). The detailed preparation process can be found in Ref. 24.

For metallographic observation and phase identification, samples were sectioned from the as-cast rods and polished to fine finish (2.5-μm diamond suspension) then etched in mixed 1:3 HF:HNO<sub>3</sub> solution for 15 s. The microstructure was characterized by optical microscopy (OM, Olympus BX-60M) and scanning electron microscopy (SEM, Sirion) coupled with energy-dispersive spectroscopy (EDS) and electron backscatter diffraction (EBSD). Phase identification was carried out by x-ray diffraction (XRD) analysis (D8 Discover) with Cu K<sub>α</sub> radiation (λ = 0.154 nm). The phase structure was analyzed by field-emission transmission electron microscopy (FE-TEM, JEM-2100F). The compressive properties of samples at room temperature were tested by using an electronic universal testing machine (CMT5105, SANS, China) at strain rate of 10<sup>-3</sup> s<sup>-1</sup>.

### RESULTS AND DISCUSSION

Figure 1 depicts the XRD patterns obtained for the FeCoNiCr<sub>0.5</sub>Al<sub>x</sub> HEAs. As the atomic ratio of Al was increased from 0.6 to 1.2, the intensity of peaks indicating the FCC solid-solution phase decreased while those corresponding to the BCC solid-solution phase increased. In the FeCoNiCr<sub>0.5</sub>Al<sub>1.2</sub> HEA,

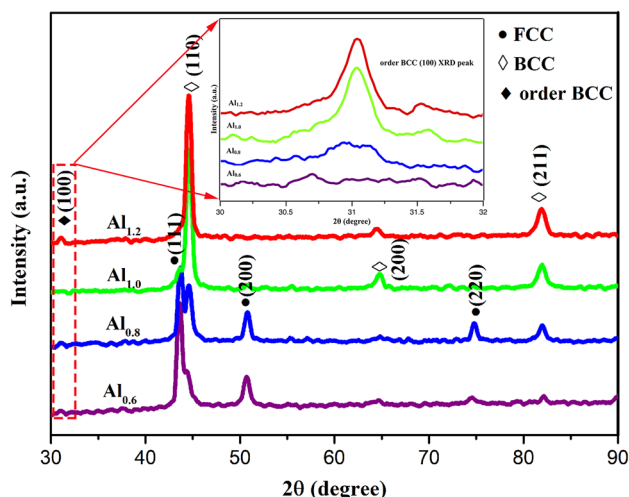


Fig. 1. XRD patterns of FeCoNiCr<sub>0.5</sub>Al<sub>x</sub> HEAs; inset shows (100) peaks obtained at low scan rate.

peaks for ordered BCC phases were detected. Obviously, all the HEAs showed dual-phase nature, but the BCC/FCC ratio increased with increasing Al addition, consistent with Ref. 25.

Figure 2 shows the compressive properties and as-cast microstructure of the FeCoNiCr<sub>0.5</sub>Al<sub>x</sub> HEAs. For the FeCoNiCr<sub>0.5</sub>Al<sub>0.6</sub> HEA, the yield strength, fracture strength, and fracture strain were 412 MPa, 2112 MPa, and 42%, respectively. The as-cast microstructure of the FeCoNiCr<sub>0.5</sub>Al<sub>0.6</sub> HEA clearly showed a dendrite of FCC solid solution with BCC-type precipitates located interdendritically, according to the XRD result above. As the Al content was increased, the matrix of the HEA changed from FCC to BCC solid solution, leading to a considerable promotion of the compressive strength. Specifically, the yield strength and fracture strength of the FeCoNiCr<sub>0.5</sub>Al<sub>0.8</sub> and FeCoNiCr<sub>0.5</sub>Al<sub>1.0</sub> HEAs were 1214 MPa, 1140 MPa, and 2923 MPa, and 2873 MPa, respectively. Meanwhile, the fracture strain in both HEAs remained at 37% and 31%, respectively. Comparing the two kinds of as-cast microstructure, the distinct difference is the volume fraction and morphology of the interdendritic phases. In the FeCoNiCr<sub>0.5</sub>Al<sub>0.8</sub> HEA, the interdendritic phase shows plate-like morphology and its volume fraction is comparable to that of the dendritic phase. However, the FeCoNiCr<sub>0.5</sub>Al<sub>1.2</sub> HEA showed brittle fracture behavior with fracture strain of 16% and decreased fracture strength of 1832 MPa.

Considering the high compressive properties of both the FeCoNiCr<sub>0.5</sub>Al<sub>0.8</sub> and FeCoNiCr<sub>0.5</sub>Al<sub>1.0</sub> HEA, the detailed morphology of their as-cast microstructures is shown in Fig. 3. Three distinct solidification structures can be found in the FeCoNiCr<sub>0.5</sub>Al<sub>0.8</sub> HEA (Fig. 3a), viz. dendrites, network-like eutectics, and plate-like eutectics. From the magnified figure of the dendrite, it is clear that rod-like nanoparticles with average size of 100 nm precipitated homogeneously in the matrix. Meanwhile, network-like eutectics appeared in the interdendritic area; the formation mechanism can be

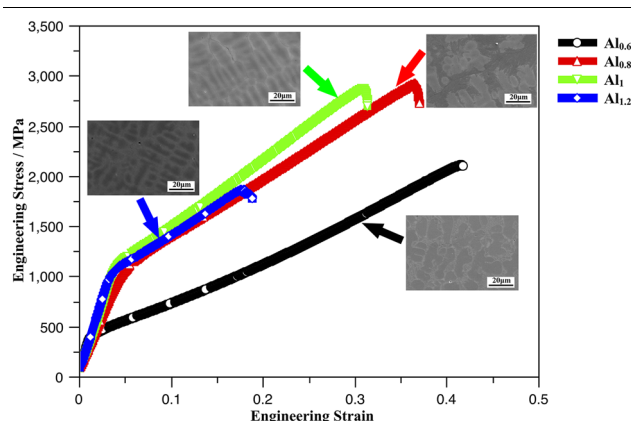


Fig. 2. Compressive stress–strain curves of FeCoNiCr<sub>0.5</sub>Al<sub>x</sub> HEAs; insets show the as-cast microstructure of each alloy.

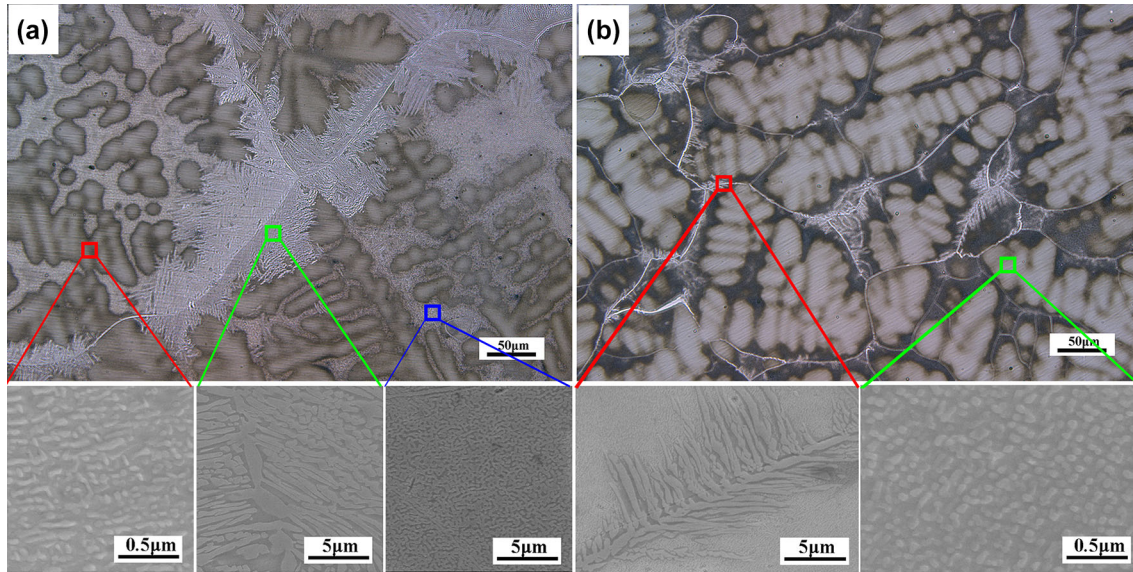


Fig. 3. As-cast microstructure of (a) FeCoNiCr<sub>0.5</sub>Al<sub>0.8</sub> and (b) FeCoNiCr<sub>0.5</sub>Al<sub>1.0</sub> HEAs; insets show magnifications of dendrites and eutectics.

characterized by the regular eutectic. Furthermore, another kind of plate-like eutectic is observed, located in grain-boundary areas. The growth direction of the plate-like eutectics was along the grain boundary and towards the grain interior. The as-cast microstructure of the FeCoNiCr<sub>0.5</sub>Al<sub>1.0</sub> HEA (Fig. 3b) was basically identical to that of the FeCoNiCr<sub>0.5</sub>Al<sub>0.8</sub> HEA. However, the volume fraction of the plate-like and network-like eutectics was remarkably decreased. For both HEAs, the BCC dendrites obviously dominated the high compressive strength performance. It is reasonable to attribute the improved ductility of this kind of dual-phase HEA to the eutectics formed both interdendritically and at grain boundaries, which considerably reduce the embrittlement of the interfaces. Meanwhile, the reduced volume fraction of the eutectics in the FeCoNiCr<sub>0.5</sub>Al<sub>1.0</sub> HEA led to a slight decrease of the compressive strain, which confirms the above deduction.

TEM images of the dendrite (Fig. 4a) and plate-like eutectics (Fig. 4b) of the FeCoNiCr<sub>0.5</sub>Al<sub>0.8</sub> HEA are shown in Fig. 4. In Fig. 4a, the selective-area electron diffraction (SEAD) patterns of nanoparticles and matrix, respectively, indicate that the dendrite matrix is an ordered BCC solid-solution phase while the nanoparticle is a disordered one. The EDS mapping results shown on the right in Fig. 4a reveal that the matrix of the dendrite was enriched in Al, Co, and Ni elements but contained less Fe and Cr. According to the detailed EDS results summarized in Table I, the ordered BCC matrix may have a (CoNi)Al-type structure. The nanoparticles, however, maintained a multicomponent distribution with high content of Al element. The EDS mapping results in Fig. 4b indicate a strong Al-enriched distribution at the interplate

area that causes the plate phase in the eutectics to be Al poor and the component ratio close to that of FeCoNiCr-based FCC solid solution, as also confirmed by the SAED pattern of the plate phase. In the interplate phase, the Al content is much higher than that in the FCC plate and the SAED pattern indicates that it has a BCC solid-solution structure. Combining the EDS results in Table I, it can be presumed that the interplate BCC phase may have (CoNi)<sub>3</sub>Al-type structure and the formation mechanism of this kind of FCC/BCC eutectics follows faceted–nonfaceted growth.

With the purpose of discussing the formation of the as-cast microstructure in the FeCoNiCr<sub>0.5</sub>Al<sub>0.8</sub> HEA, the phase diagram of the FeCoNiCr<sub>0.5</sub>Al<sub>x</sub> HEA was calculated with the aid of Pandat software (CompuTherm, USA) using the PanHEA database (Fig. 5). A ternary-phase region and a quaternary-phase region are located below the binary-phase region of B2 + Liquid. As the FeCoNiCr<sub>0.5</sub>Al<sub>0.8</sub> HEA solidifies, the first phase formed is B2-type BCC phase, which has a dendrite morphology as shown in Fig. 3. However, due to the strong interaction between Al and other transitional elements, a spinodal decomposition process takes place, forming BCC nanoprecipitates in the matrix.<sup>26</sup> Then, a eutectic reaction occurs interdendritically to form the network-like eutectics as the temperature of the melt decreases into the ternary-phase region. As this reaction proceeds, residual liquid will continue to be pushed to grain boundaries, and the content changes along the line below the B2 + Liquid binary-phase region, heading towards the quaternary-phase region. Finally, another eutectic reaction occurs at the grain boundary to form the plate-like eutectics. The complex as-cast microstructure in the dual-phase FeCoNiCr<sub>0.5</sub>Al<sub>0.8</sub> HEA can be



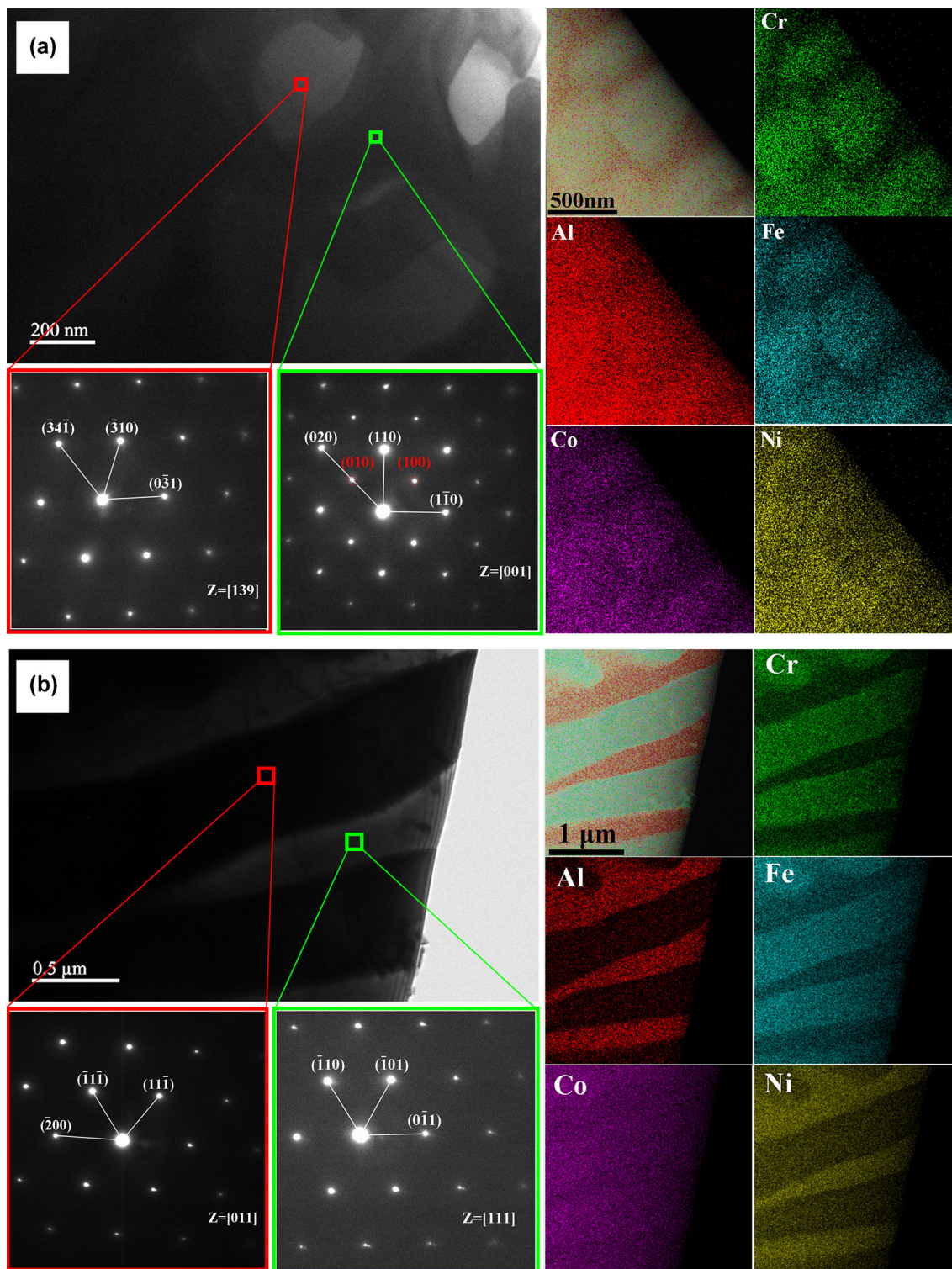
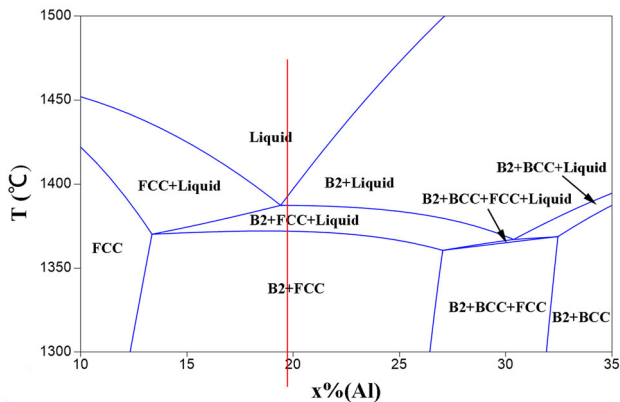


Fig. 4. TEM images, SAED patterns, and EDS maps of (a) dendrite phase and (b) plate-like eutectics in FeCoNiCr<sub>0.5</sub>Al<sub>0.8</sub> HEA.

**Table I. EDS results (at.%) for dendrite phase and plate-like eutectics**

Phase and state	Fe	Co	Ni	Cr	Al
Dendrite					
Overall	16.03	15.48	12.42	8.80	47.27
Matrix	12.52	14.88	17.13	4.97	50.50
Precipitates	18.92	16.29	10.24	11.59	42.96
Plate-like eutectics					
Overall	26.59	26.16	22.05	16.10	9.10
Plate	30.78	27.14	17.88	19.93	4.26
Interplate	19.73	24.63	29.31	8.79	17.53

Fig. 5. Phase diagram of FeCoNiCr<sub>0.5</sub>Al<sub>x</sub> HEAs calculated using Pandat software.

explained based on the results and discussion above. Meanwhile, it can be concluded that the formation of eutectics with distinct morphology can be attributed to the Al content in the residual liquid.

## CONCLUSION

FeCoNiCr<sub>0.5</sub>Al<sub>x</sub> HEAs were prepared via the self-propagating high-temperature casting method and their as-cast microstructures and formation mechanism systematically investigated. Based on the results and discussion, the following conclusions can be drawn:

1. The FeCoNiCr<sub>0.5</sub>Al<sub>x</sub> HEAs showed dual-phase nature with complex as-cast microstructure depending on the Al content.
2. The as-cast microstructure of the FeCoNiCr<sub>0.5</sub>Al<sub>0.8</sub> and FeCoNiCr<sub>0.5</sub>Al<sub>1.0</sub> HEAs was composed of ordered/nonordered BCC nanocomposite dendrites, network-like interdendritic FCC/BCC eutectics, and plate-like FCC/BCC eutectics.
3. The compressive yield strength, fracture strength, and strain of the FeCoNiCr<sub>0.5</sub>Al<sub>0.8</sub> HEA were 1214 MPa, 2923 MPa, and 37%,

being much higher than the values for the other HEAs. These high compressive properties can be attributed to the eutectics formed both inter-dendritically and at grain boundaries, which considerably reduce the embrittlement of the interfaces.

## ACKNOWLEDGEMENTS

This work was supported by the National Natural Science Foundation of China (Grant No. 51671056), Jiangsu Key Laboratory for Advanced Metallic Materials (Grant No. BM2007204), and Fundamental Research Funds for the Central Universities (Grant No. 2242019K40271). We thank CompuTherm LLC, USA, for support in the form of the HEA thermodynamic database and advice regarding the computing process.

## REFERENCES

1. J.W. Yeh, S.K. Chen, S.J. Lin, J.Y. Gan, T.S. Chin, T.T. Shun, C.H. Tsau, and S.Y. Chang, *Adv. Eng. Mater.* 6, 299 (2004).
2. B. Cantor, *Entropy* 16, 4749 (2014).
3. Z.W. Wang, I. Baker, W. Guo, and J.D. Poplawsky, *Acta Mater.* 126, 346 (2017).
4. P.P. Li, A.D. Wang, and C.T. Liu, *Intermetallics* 87, 21 (2017).
5. Y.N. Sun, P. Chen, L.H. Liu, M. Yan, X.Y. Wu, C.Y. Yu, and Z.Y. Liu, *Intermetallics* 93, 85 (2018).
6. N.D. Stepanov, D.G. Shaysultanov, G.A. Salishchev, M.A. Tikhonovskiy, E.E. Oleynik, A.S. Tortika, and O.N. Senkov, *J. Alloys Compd.* 628, 170 (2015).
7. R. Agarwal, R. Sonkusare, S.R. Jha, N.P. Gurao, K. Biswas, and N. Nayan, *Mater. Des.* 157, 539 (2018).
8. B. Gludovatz, A. Hohenwarter, D. Catoor, E.H. Chang, E.P. George, and R.O. Ritchie, *Science* 345, 1153 (2014).
9. J.Y. He, C. Zhu, D.Q. Zhou, W.H. Liu, T.G. Nieh, and Z.P. Lu, *Intermetallics* 55, 9 (2014).
10. M.D. Alcala, C. Real, I. Fombella, I. Trigo, and J.M. Corbella, *J. Alloys Compd.* 749, 834 (2018).
11. B. Wang, J. Huang, J.H. Fan, Y.P. Dou, H. Zhu, and D.H. Wang, *J. Electrochem. Soc.* 164, E575 (2017).
12. S.G. Ma, S.F. Zhang, M.C. Gao, P.K. Liaw, and Y. Zhang, *JOM* 65, 1751 (2013).
13. S.Q. Xia, X. Yang, T.F. Yang, S. Liu, and Y. Zhang, *JOM* 67, 2340 (2015).
14. Y. Zhang, Y.J. Zhou, J.P. Lin, G.L. Chen, and P.K. Liaw, *Adv. Eng. Mater.* 10, 534 (2008).
15. S. Guo and C.T. Liu, *Prog. Nat. Sci.* 21, 433 (2011).
16. D.B. Miracle and O.N. Senkov, *Acta Mater.* 122, 448 (2017).
17. I. Basu, V. Ocelik, and J.T. De Hosson, *Acta Mater.* 157, 83 (2018).
18. G.Y. Ke, S.K. Chen, T. Hsu, and J.W. Yeh, *Ann. Chim. Sci. Mater.* 31, 669 (2006).
19. Y. Ma, Y.H. Feng, T.T. Debela, G.J. Peng, and T.H. Zhang, *Int. J. Refract. Met. Hard Mater.* 54, 395 (2016).
20. J. Wang, S.Z. Niu, T. Guo, H.C. Kou, and J.S. Li, *J. Alloys Compd.* 710, 144 (2017).
21. J.Y. He, H. Wang, H.L. Huang, X.D. Xu, M.W. Chen, Y. Wu, X.J. Liu, T.G. Nieh, K. An, and Z.P. Lu, *Acta Mater.* 102, 187 (2016).
22. T. Yang, Y.L. Zhao, Y. Tong, Z.B. Jiao, J. Wei, J.X. Cai, X.D. Han, D. Chen, A. Hu, J.J. Kai, K. Lu, Y. Liu, and C.T. Liu, *Science* 362, 933 (2018).
23. J.T. Fan, L.J. Zhang, P.F. Yu, M.D. Zhang, G. Li, P.K. Liaw, and R.P. Liu, *Scr. Mater.* 159, 18 (2019).
24. T. Lu, W.K. Chai, Y. Pan, T. Dai, and D.K. Sun, *Metall. Mater. Trans. B Process. Metall. Mater. Process. Sci.* 50, 32 (2019).

25. C. Zhang, F. Zhang, H.Y. Diao, M.C. Gao, Z. Tang, J.D. Poplawsky, and P.K. Liaw, *Mater. Des.* 109, 425 (2016).
26. Q. Wang, Y. Ma, B.B. Jiang, X.N. Li, Y. Shi, C. Dong, and P.K. Liaw, *Scr. Mater.* 120, 85 (2016).

**Publisher's Note** Springer Nature remains neutral with regard to jurisdictional claims in published maps and institutional affiliations.